Radial Packing, Order, and Disorder in Collagen Fibrils

David J. S. Hulmes,* Tim J. Wess,* Darwin J. Prockop,‡ and Peter Fratzl§

*Department of Biochemistry, University of Edinburgh, George Square, Edinburgh EH8 9XD, United Kingdom; ‡Department of Biochemistry and Molecular Biology, Thomas Jefferson University, Philadelphia, Pennsylvania 19107 USA; and §Department of Mathematics, Heriot-Watt University, Riccarton, Edinburgh EH14 4AS United Kingdom

ABSTRACT Collagen fibrils resemble smectic, liquid crystals in being highly ordered axially but relatively disordered laterally. In some connective tissues, x-ray diffraction reveals three-dimensional crystallinity in the molecular packing within fibrils, although the continued presence of diffuse scatter indicates significant underlying disorder. In addition, several observations from electron microscopy suggest that the molecular packing is organized concentrically about the fibril core. In the present work, theoretical equatorial x-ray diffraction patterns for a number of models for collagen molecular packing are calculated and compared with the experimental data from tendon fibrils. None of the models suggested previously can account for both the crystalline Bragg peaks and the underlying diffuse scatter. In addition, models in which any of the nearest-neighbor, intermolecular vectors are perpendicular to the radial direction are inconsistent with the observed radial orientation of the principal ~4 nm Bragg spacing. Both multiple-start spiral and concentric ring models are devised in which one of the nearest-neighbor vectors is along the radial direction. These models are consistent with the radial orientation of the ~4 nm spacing, and energy minimization results in radially oriented crystalline domains separated by disordered grain boundaries. Theoretical x-ray diffraction patterns show a combination of sharp Bragg peaks and underlying diffuse scatter. Close agreement with the observed equatorial diffraction pattern is obtained. The concentric ring model is consistent with the observation that the diameters of collagen fibrils are restricted to discrete values.

INTRODUCTION

Collagen fibrils are the principal, tensile stress-bearing components of connective tissues. Fibrils form by self-assembly of collagen molecules, where the fibril-forming collagens (types I, II, III, V, and XI) constitute a subfamily from at least 18 different types of collagens in vertebrates (van der Rest and Garrone, 1991; Hulmes, 1992; Mayne and Brewton, 1993). In general, according to age, collagen type composition, and tissue source, fibrils are approximately cylindrical, with diameters in the range of 10–500 nm (Parry and Craig, 1984). Fibrils are frequently organized into bundles or lamellae, and the size and higher-order arrangement of fibrils gives rise to tissue-specific, biomechanical, and other biological properties (Birk and Linsenmayer, 1994).

Within a fibril, there is considerable long-range order in the axial direction, with neighboring collagen molecules staggered axially by integral multiples of D (i.e., nD, $n = 1$, 2, 3, or 4, where D ~ 67 nm, depending on tissue source; Brodsky and Eikenberry, 1982). The lateral arrangement of molecules (i.e., in a plane perpendicular to the fibril axis) is less well established. In the fibrils from some tissues, x-ray diffraction indicates only liquid-like short-range order in the lateral packing, as shown by the diffuse equatorial scattering (i.e., perpendicular to the fibril axis) with a maximum in the region of the intermolecular interference function (Woodhead-Galloway and Machin, 1976; Grynpas, 1977; Brodsky and Eikenberry, 1982; Fratzl et al., 1993). In addition, there is evidence from nuclear magnetic resonance for considerable azimuthal mobility (i.e., rotation of molecules about their axes) within fibrils (Jelinski et al., 1980; Torchia, 1982). Such an arrangement, with long-range order in the axial direction but only short-range order in the lateral direction, has been likened to that of a smectic A liquid crystal (Hukins and Woodhead-Galloway, 1977).

In the equatorial x-ray diffraction patterns from some fibrils, e.g., rat tail tendon (Miller, 1976), other tendons (Jesior et al., 1980), or lamprey notochord (Eikenberry et al., 1984), superimposed on the underlying diffuse scatter is a set of sharp Bragg reflections that have been indexed in terms of a three-dimensional triclinic unit cell that arises from quasi-hexagonal crystalline molecular packing (Hulmes and Miller, 1979; Fraser et al., 1983). Compressed microfibril models have also been proposed (Piez and Trus, 1981), although with the same unit cell, the difference being the assignment of molecular segments within the unit cell (Fraser et al., 1987; Jones and Miller, 1991). Whatever the unit cell contents, the principal equatorial lattice spacings are at ~3.8 and 2.6 nm. The presence of systematic deviations between observed and ideal lattice positions indicates the presence of distortion due to curvature (Fraser et al., 1983). Using x-ray diffraction to monitor structural preservation during

Received for publication 8 August 1994 and in final form 30 January 1995.

Address reprint requests to Dr D.J.S. Hulmes, Department of Biochemistry, University of Edinburgh, Hugh Robson Building, George Square, Edinburgh EH8 9XD UK. Tel.: 44-1 31-650-3731; Fax: 44-1 31-650-3711; E-mail: djsh@srvl.med.ed.ac.uk.

Peter Fratzl's permanent address is Institut für Festkörperphysik der Universität Wien and Ludwig-Boltzmann Institut für Osteologie, Strudlhofg. 4, A-1090 Wien, Austria.

Tim Wess's current address is Department of Biological and Molecular Sciences, University of Stirling, Stirling FK9 4LA, UK.

0006-3495/95/05/1661/10 $2.00

specimen preparation for electron microscopy, Hulmes et al. (1981, 1985) found in transverse sections of collagen fibrils that the largest lattice spacing is preferentially oriented in a radial direction with evidence of both lattice curvature and discontinuities between adjacent crystalline domains.

In addition to the observed radial orientation of the crystalline domains, there is further evidence from electron microscopy for a concentric organization in collagen fibrils from various sources. This includes a number of reports of a distinct fibril core (Luft, 1971; Nakao and Bashey, 1972; Franc, 1993) and numerous observations of a helicoidal arrangement in the molecular packing, as revealed by freeze-fracture (Ruggeri et al., 1979; Raspanti et al., 1989; Katsura et al., 1991). It has also been observed that the diameters of collagen fibrils in relatively young animals show discrete increments of ~8 nm (Parry and Craig, 1984), and this is most readily interpreted in terms of incremental growth in concentric 4 nm thick layers (Hulmes, 1983).

To understand fully the molecular packing in collagen fibrils, models must clearly take account of both the short-range (liquid-like) and long-range (crystalline) order in the lateral molecular packing. The models proposed previously to account for the x-ray diffraction data have focused on only one of these aspects, i.e., the crystalline packing or the liquid-like packing. Here we consider a number of concentric and spiral packing arrangements in the light of experimental data from both x-ray diffraction and electron microscopy. We show that the concentric structures so far proposed (Galloway, 1985; Silver et al., 1992) are inconsistent with the observed equatorial x-ray diffraction pattern. Furthermore, models with long-range order in which any of the nearest-neighbor vectors are directed circumferentially are inconsistent with the observed radial orientation of the 3.8 nm spacing, which requires that one of the nearest-neighbor vectors be directed radially (see below). We devise new concentric ring and spiral models with radial nearest-neighbor contacts that show, after energy minimization, features of both liquid-like and crystalline order. For the first time, all aspects of the observed equatorial x-ray diffraction data were taken into account in modeling the structure.

THEORY AND METHODS

Fibril dimensions

All calculations were done on fibril cross sections constructed to a diameter of 100 nm. As a result of the non-integral relation between the molecular length (~4.5 D) and the D spacing, fibrils consist of alternating regions of high packing density (overlap region) and low packing density (gap region) where the ratio of packing densities is 0.8. Typically each fibril contained 3800–4000 molecules in a cross section of the overlap region, with each molecular cross section represented as a disc of diameter 1.08 nm (see below).

Energy minimization

In some cases, energy minimization of the molecular coordinates was performed to relax the structures, as follows. A Lennard-Jones (L-J) interaction potential (U), containing both repulsive (short-range) and attractive (long-range) components, was defined as

$$U = 4\,\epsilon\,\Sigma_{i,j}\,[(\sigma/r_{i,j})^{12} - (\sigma/r_{i,j})^{6}]$$

where $\sigma = 1.376$ nm, $kT/\epsilon = 0.39$, k is the Boltzmann factor, and T is the absolute temperature. The sum extends over all pairs of molecules (i,j), and $r_{i,j}$ is the distance between the molecules in the equatorial plane. The value of σ was chosen in such a way that the potential was a minimum for a distance r given by

$$r = \sigma\,2^{(1/6)} = 1.545\ \text{nm}$$

which approximates to the nearest-neighbor intermolecular spacing in the quasi-hexagonal packing scheme (Hulmes and Miller, 1979). In a typical model, the number of molecules per unit area (r) in the overlap region was ~0.5 nm^{-2}, in accordance with the experimentally observed packing density (Hulmes and Miller, 1979), therefore the dimensionless quantity $\rho\sigma^2$ was about 0.95. This situates the minimum of the L-J potential within the region of stability for the solid phase (Abraham, 1981). To preserve the pre-existing structures as much as possible and to remove only very improbable configurations (e.g., molecular overlaps), we wanted the parameter kT/ϵ to be as small as possible. Making it too small, however, would not have allowed the molecules to move at all. After a few trials, we chose the smallest possible value, where the ratio of actual to attempted moves was reasonably large (~1 in 2).

Computer simulations were performed using a program written for standard applications of L-J potentials and adapted for the present purpose. In this program, based on a standard algorithm (Abraham, 1981), the positions of all molecules were stored in an array. At each step, a molecule was chosen at random and moved in a random direction. The length of the move was also randomly distributed, in the range 0–0.8 nm, i.e., smaller than the equilibrium distance between nearest-neighbor molecules. This prevented molecules from "jumping over" each other, which would be unrealistic given that the axial arrangement of molecules is well defined. The change in potential energy of the system (δU) associated with the move was then calculated by (calling I the molecule chosen for a move)

$$\delta U = 4\epsilon\,\Sigma_j\,[(\sigma/r'_{I,j})^{12} - (\sigma/r_{I,j})^{12} - (\sigma/r'_{I,j})^{6} + (\sigma/r_{I,j})^{6}]$$

where $r'_{I,j}$ refers to distances after the move. According to the Metropolis rule (Abraham, 1981), the move was performed (i.e., the array of molecular positions was updated), if δU was negative. If δU was positive, the move was performed only with probability $e^{(-\delta U/kT)}$. After each move the procedure was started again. Runs were performed with an average of 50 attempted moves per molecule (i.e., a total of ~4 × 108

calculations of pair interaction energies), taking ~8 h on a Sparc workstation. At the end of the run, all unfavorable interactions, i.e., molecular overlaps, had been removed, although the structure had not reached an overall energy minimum.

Fourier transformation

All structures were subjected to two-dimensional Fourier transformation, for comparison of rotationally averaged theoretical intensities (i.e., squared amplitudes) with the observed equatorial x-ray diffraction profile. The intensity at each radial position R in the rotationally averaged transform, $I(R)$, was calculated by multiplying the rotationally averaged squared modulus of the interference function by an intensity form factor $F(R)$, as follows

$$I(R) = < | \Sigma_n e^{2\pi i(x_n X + y_n Y)} |^2 > F(R)$$

where R is the reciprocal space radial coordinate at position (X,Y); x_n and y_n are the coordinates of the axis (in cross section) of the *nth* molecule in the model, and < > represents rotational averaging. $F(R)$ is the intensity form factor of a cylinder of diameter D = 1.08 nm, which is a good approximation to the equatorial scattering from the collagen triple helix (Fratzl et al., 1993), given by

$$F(R) = [2 J_1(\pi RD)/\pi RD]^2$$

where J_1 is the first-order Bessel function. The interference function was calculated in X,Y increments of 0.005 nm^{-1}, from 0 to 1 nm^{-1} in reciprocal space, and then rotationally averaged by summing intensity values in concentric shells of width 0.01 nm^{-1} and dividing the total for each shell by the number of data points.

Separate contributions to the theoretical x-ray scattering profile were calculated for the gap and overlap regions. Gap regions were derived from overlap regions by deletion of 1/5 of the molecules, leaving the coordinates of the remaining molecules unchanged. All molecules were weighted equally in the Fourier transforms. Unless otherwise stated theoretical profiles for hybrid structures (e.g., gap and overlap) were calculated by adding individual transforms coherently in the complex plane, i.e., before calculation of the squared modulus and rotational averaging.

Experimental data

X-ray diffraction patterns of native rat tail tendon were obtained at beamline 7.2 at the Synchrotron Radiation Source, Daresbury Laboratory (Cheshire, UK). The near-equatorial scattering in the Z-range 0–0.1 nm^{-1} was projected onto Z = 0 (the equator), for comparison with the theoretical scattering profiles. No correction was made for curvature of the Ewald sphere, this being <1% at R = 0.1 nm^{-1}. Furthermore, no polarization correction was applied, as only (near) equatorial data were considered.

RESULTS AND DISCUSSION

Crystalline order and liquid-like disorder

The starting points for the development of fibril models were the two extremes of order as illustrated by crystalline, quasi-hexagonal packing (Fig. 1) and liquid-like disorder (Fig. 2).

In Fig. 1, unit cell dimensions and molecular coordinates in the overlap (Fig. 1 *a*) and gap (Fig. 1 *b*) regions are from Fraser et al. (1983), and the fibril is a single crystalline array with shape arbitrarily defined by a circle of radius 50 nm. As expected, only sharp peaks (Bragg reflections) are observed in the theoretical equatorial diffraction patterns (Fig. 1, *c*, *d*, and *e*), at positions corresponding to the observed Bragg reflections (Fig. 1 *f*). Most of the contrast at low resolution is provided by the gap region (Fig. 1 *d*), since the height of the low-angle maxima in relation to the peaks at 0.75 to 0.79 nm^{-1} is greater than for the overlap region (Fig. 1c). The underlying diffuse scatter in the experimental data (Fig. 1f), which rises to a broad maximum in the region of 0.77 nm^{-1}, is not accounted for by the single crystal model.

In Fig. 2 *a*, molecular coordinates were generated using a hard disc (HD) model for liquid-like packing, with the same packing density (0.485 molecules nm^{-2} in the overlap region) as the quasi-hexagonal lattice (Fig. 1), and a repulsion diameter of 1.2 nm. As shown earlier (Woodhead-Galloway and Machin, 1976), such a model gives reasonable agreement with the observed diffuse scattering profile without the crystalline Bragg reflections, and accounts quantitatively, e.g., for the scattering from turkey leg tendon at varying degrees of hydration (Fratzl et al., 1993). In the HD liquid model, molecules can move freely with the only restriction that they must not overlap. Fig. 2 *b* shows such a liquid structure for the gap region, with the packing density reduced by 1/5 with respect to Fig. 2 *a* (i.e., 0.388 molecules nm^{-2}). (Note that this is not the same as removing 1/5 of the molecules in Fig. 2 *a* at random, as this does not account properly for the correlations in position imposed only by the non-overlap condition of the molecules.) The x-ray scattering calculated for the configurations in Fig. 2, *a* and *b* are shown in Fig. 2, *c* and *d*, respectively. Apart from the noise (due to the comparatively small number of molecules considered) the curves correspond to the well-known diffuse maxima as calculated, e.g., in the Percus-Yevick approximation (Woodhead-Galloway and Machin, 1976). Fig. 2 *e* shows the combined x-ray scattering as estimated for an HD liquid structure in both the gap and overlap regions, which accounts for the diffuse component in the measured x-ray scattering from rat tail tendon (Fig. 2 *f*), but not for the observed Bragg peaks.

We examined the possibility that long-range two-dimensional order could be introduced into the HD packing model by assignment of axial staggers simply according to their distance from the fibril axis. The rationale for this came from the work of Chapman (1989), who proposed that molecules are in liquid-like array in cross section, but with one molecular segment (e.g., segment 1; Hulmes and Miller,

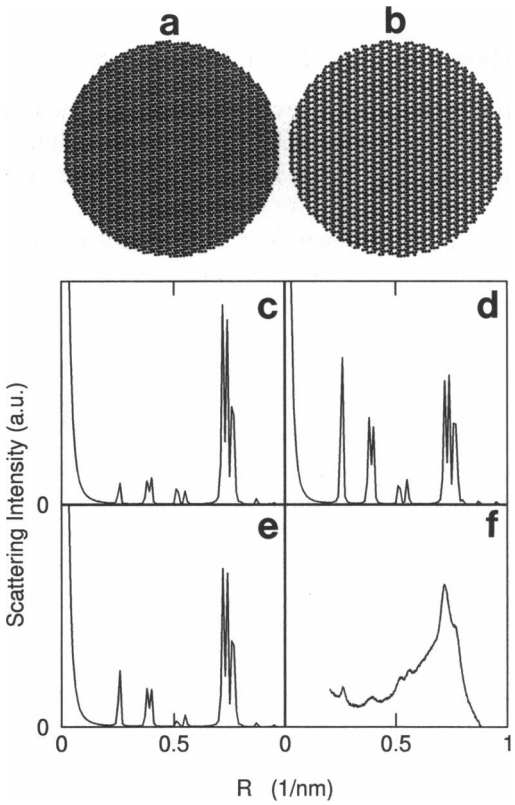

FIGURE 1 Single crystal model for molecular packing in collagen fibrils. Molecules in cross section, indicated by solid circles, are arranged on a quasi-hexagonal lattice, with unit cell dimensions and lateral molecular coordinates from Fraser et al. (1983). As in subsequent models, a fibril of diameter 100 nm is shown in (*a*) the overlap region and (*b*) the gap region, with corresponding rotationally averaged theoretical scattering intensity profiles in (*c*) and (*d*), respectively. The predicted scattering profile for the combined gap/overlap structure is shown in (*e*), with the observed equatorial x-ray diffraction pattern from rat tail tendon in (*f*). Calculated scattering profiles are on the same absolute scale.

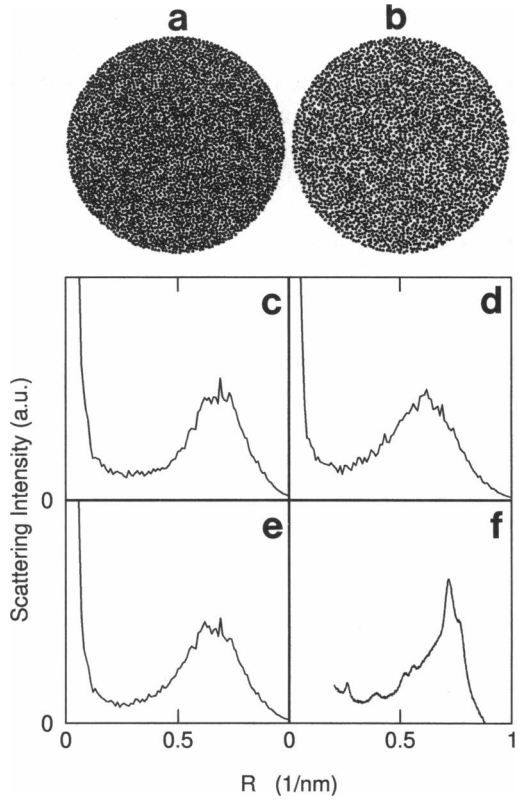

FIGURE 2 HD liquid model for molecular packing in collagen fibrils. Molecules in cross section, indicated by solid circles, are arranged with a packing density of 0.485 molecules nm^{-2} (as in the quasi-hexagonal lattice) in the overlap region (*a*) and 0.388 molecules nm^{-2} in the gap region (*b*). All molecules in the gap region share identical coordinates with corresponding molecules in the overlap region. Rotationally averaged theoretical scattering intensity profiles for the overlap and gap regions are shown in (*c*) and (*d*), respectively. The predicted scattering profile for the combined gap/overlap structure is shown in (*e*), with the observed equatorial x-ray diffraction pattern in (*f*). Calculated scattering profiles are on the same absolute scale.

1979) confined to the surface of the fibril due either to retention of *N*-propeptides or to interactions with proteoglycans. In the next D repeat, molecules with segment 1 in the first D repeat will have their segments 2 somewhat closer to the axis of the fibril, as the segments 1 from a different set of molecules will now be surface located, and so on. In this way, molecular segments in cross section would increment systematically with radial position. We therefore assigned each segment number (s) according to the rule

$$s = \mathrm{MOD}\{[\mathrm{INT}(5r/d)]/5\} + 1$$

where r is the radial position, and $d = 3.778$ nm; INT represents the truncated integer, and MOD represents the remainder (between 0 and 4) after dividing INT($5r/d$) by 5. When Fourier transformed (not shown), the imposed one-dimensional order appeared as peaks at multiples of (1/3.778) nm^{-1}, but two-dimensional order did not appear. Therefore, to account for all the features of the observed equatorial x-ray scattering profile, a combination of two-dimensional crystalline order (Fig. 1) and short-range liquid-like order (Fig. 2) is required.

Previous concentric models

Ramachandran and Sasisekharan (1956) and Sasisekharan and Ramachandran (1957) described both cylindrical and spiral models for the molecular packing in collagen fibrils. These authors calculated scattering profiles and rotationally averaged optical transforms for comparison with the observed equatorial x-ray diffraction pattern from tendon. A combination of principal maxima and subsidiary maxima was predicted, with a principal maximum in the region of 0.74–0.79 nm^{-1}, as observed. The positions of the subsidiary maxima showed some agreement with the observed data, although a number of predicted peaks were not observed, particularly in comparison with more recent data (Hulmes and Miller, 1979). It is important to note that the work of Ramachandran and Sasisekharan took no account of the relative axial staggers between molecules, and it was before the existence of gap and overlap regions was first recognized (Hodge and Petruska, 1963).

The cylindrical model was further explored by Galloway (1985), who devised a concentric layer structure in which

neighboring molecules within each layer were related circumferentially by a stagger of 1 D, with the number of molecules in layer m being 5m. The intermolecular spacing (a) within each layer was fixed at 1.595 nm, and the interlayer spacing (d) converged asymptotically from 1.357 nm (innermost layer) to 1.269 nm, when $2\pi d/a = 5$. Fig. 3 shows this structure in both the overlap and gap regions, with corresponding theoretical equatorial scattering profiles. While the structure of the fibril in the overlap region (Fig. 3 a) appears to be isotropic with fivefold symmetry, the gap region (Fig. 3 b) reveals a highly anisotropic structure. There is no contribution to the low-angle scattering profile (i.e., $R < 0.5$ nm^{-1}) from the overlap region (Fig. 3 c), while the gap region (Fig. 3 d) gives rise to a series of maxima at multiples of 1/5 a (i.e., $n \times 0.125$ nm^{-1}). A peak corresponding to the interlayer spacing (d) is also apparent. The agreement of the combined gap/overlap structure (Fig. 3 e) with the observed diffraction pattern (Fig. 3 f) is poor.

A cylindrical model was also developed by Silver et al. (1992) to account for the growth of fibrils with paraboloidal shaped tips (Holmes et al., 1992). In cross section, the building rules were similar to those of Galloway (1985), with neighboring molecules within each layer related circumferentially by a stagger of 1 D. In cross section, the number of molecules within each layer was again a multiple of 5, but the interlayer spacing was constant and equal to the intermolecular spacing within a layer. Additional gaps were introduced as a result of the so-called 2π problem, whereby if the intermolecular spacing (a) within a layer is equal to the interlayer spacing (d), then there is space for an additional $2\pi d/a = 2\pi$ molecules per layer, i.e., not a multiple of 5. Using the same intermolecular spacing as Galloway (1985), a model was built based on that of Silver et al. (1992), where strand continuity was maintained by jumping from one layer to the next when the number of molecules within a layer was complete (Fig. 4). Again, agreement between theoretical and observed diffraction patterns is poor.

As well as showing poor agreement with the observed x-ray diffraction data, the models of Galloway (1985) and Silver et al. (1992) also disagree with the electron microscopic data on the orientation of the 3.8 nm repeat in the

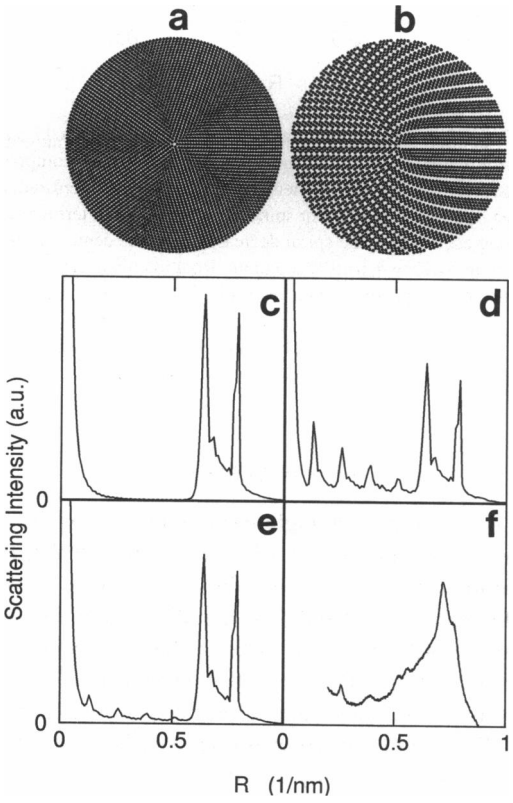

FIGURE 3 Cylindrical model of Galloway (1985). Molecules are arranged in concentric layers, with a constant intermolecular spacing within each layer (measured along the chord) of 1.595 nm. The interlayer spacing converges asymptotically from 1.357 to 1.269 nm, so that the number of additional molecules per layer is 5. The overlap region (a) shows fivefold symmetry, whereas the gap region (b) is highly anisotropic. Rotationally averaged theoretical scattering intensity profiles for the overlap and gap regions are shown in (c) and (d), respectively. The predicted scattering profile for the combined gap/overlap structure is shown in (e), with the observed equatorial x-ray diffraction pattern in (f). Calculated scattering profiles are on the same absolute scale.

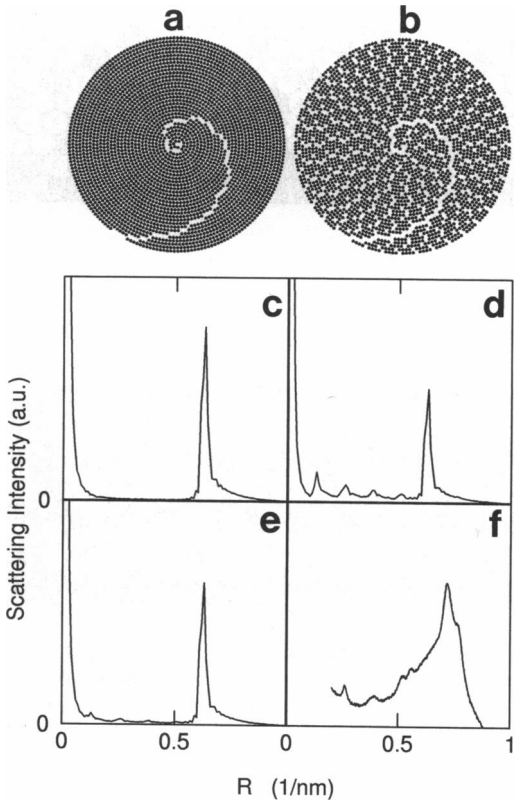

FIGURE 4 Cylindrical model of Silver et al. (1992). Molecules are arranged in concentric layers, with a constant intermolecular spacing within each layer (measured along the circumference) of 1.595 nm, equal to the interlayer spacing. Each layer contains a multiple of 5 molecules, and gaps are introduced to overcome the "2π problem" (see text). Strands of molecules in adjacent layers are continuous. Rotationally averaged theoretical scattering intensity profiles for the overlap and gap regions are shown in (c) and (d), respectively. The predicted scattering profile for the combined gap/overlap structure is shown in (e), with the observed equatorial x-ray diffraction pattern in (f). Calculated scattering profiles are on the same absolute scale.

quasi-hexagonal lattice (Hulmes et al., 1981, 1985), which shows a preferred radial direction. Within the quasi-hexagonal packing scheme, when one of the lines of molecular contacts (i.e., nearest-neighbor vector) is oriented circumferentially as in the models of both Galloway (1985) and Silver et al. (1992), it is impossible for the 3.8 nm spacing to be oriented radially, as demonstrated in Fig. 5 *a*. If one of the nearest-neighbor vectors is radial, however, then a radial orientation of the 3.8 nm repeat can be accommodated (Fig. 5 *b*).

New concentric models

We have devised both spiral and cylindrical models with radial nearest-neighbor intermolecular contacts (Figs. 6 to 9). Spiral structures were constructed with multiple starts, as illustrated for a 17-start spiral in Fig. 6. The path of each arm of the spiral was defined by

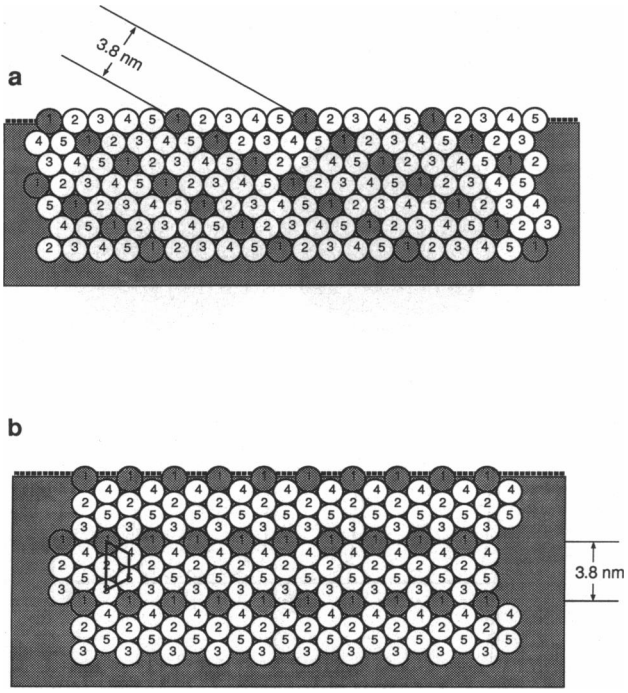

FIGURE 5 Circumferential packing versus radial packing. Molecules are arranged on a hexagonal lattice, with molecular D segments (corresponding to axial stagger positions) indicated from 1 to 5. Molecules indicated by the same molecular segment are at the same axial position within the fibril. Circumferential packing (*a*) occurs when one of the lines of molecular contacts (nearest-neighbor vectors) is parallel to the surface of the fibril (indicated by a broken line). Bragg planes corresponding to the 3.8 nm spacing in the quasi-hexagonal lattice are oriented oblique to the fibril surface. Other orientations are possible (see Fig. 3), but the 3.8 nm spacing can never be perpendicular to the surface. Radial packing (*b*) occurs when one of the lines of molecular contacts (nearest-neighbor vectors) is perpendicular to the fibril surface, i.e., directed along the radius of the fibril in cross section. The 3.8 nm spacing can now be oriented radially, as observed experimentally. Both structures can be considered as arrays of compressed microfibrils, where the outline of one such microfibril is shown in (*b*). The assignment of molecules to segments 1–5 is arbitrary. In the calculation of theoretical scattering profiles, all molecular segments are equivalent, except the segment of length ~0.5 D.

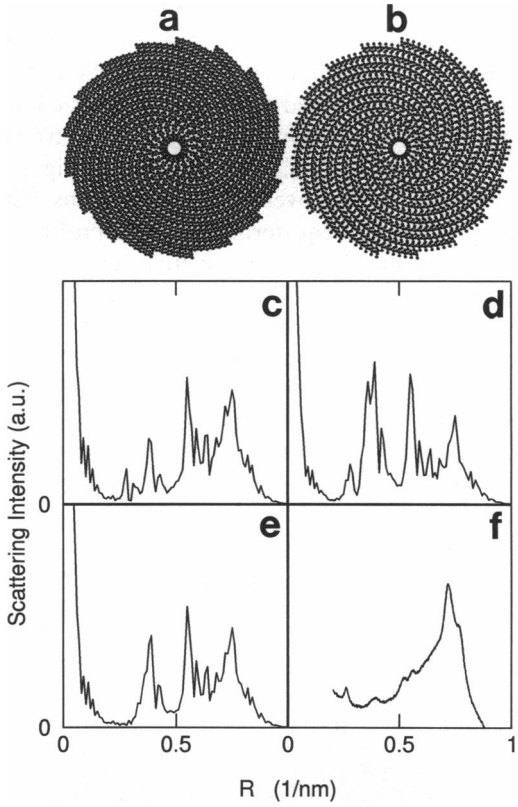

FIGURE 6 Spiral model with radial molecular packing. A 17-start spiral is shown in which each arm of the spiral is composed of compressed microfibrils, with their longest dimension (see Fig. 5) oriented radially. The radial distance between adjacent spiral arms is 3.8 nm. Intermicrofibril distance along each arm of the spiral decreases from the center of the fibril to give constant packing density throughout. Rotationally averaged theoretical scattering intensity profiles for the overlap (*a*) and gap (*b*) regions are shown in (*c*) and (*d*), respectively. The predicted scattering profile for the combined gap/overlap structure is shown in (*e*), with the observed equatorial x-ray diffraction pattern in (*f*). Calculated scattering profiles are on the same absolute scale.

$$r = Nd\theta/2\pi$$

where r is the radius at angle θ (in radians), N is the number of spiral arms, and d = 3.778 nm. Along each arm, compressed microfibrils (Piez and Trus, 1981) were placed with their longest side oriented in a radial direction, with the intermicrofibril spacing adjusted so that the packing density was constant throughout the fibril and equal to the packing density in the quasi-hexagonal lattice (Hulmes and Miller, 1979). The use of compressed microfibrils to generate such structures does not imply that the microfibril is a structural unit within the fibril; it is simply a convenient way of generating packing models with nearly radial nearest-neighbor contacts.

Theoretical scattering profiles for the 17-start spiral are shown in Fig. 6, *c–e*. Several peaks are predicted in the low-angle scattering region, and agreement with the observed profile is poor. Moreover, there are a large number of unacceptably close molecular contacts in the geometrically produced spiral structures. To eliminate these, energy minimization (relaxation) was carried out using the Lennard-Jones

potential. During the relaxation procedure, all the molecules were considered indistinguishable as depicted in the cross section through the overlap region (Fig. 7 *a*), but the axial stagger positions of each individual molecule were stored. After relaxation, one set of molecules with equivalent axial staggers was removed to generate the gap region structure in Fig. 7 *b*. Relaxation results in the spiral structure being difficult to discern in the overlap region (Fig. 7 *a*), although it remains clearly visible in the gap region (Fig. 7 *b*). In the theoretical scattering profiles, many of the peaks from the model before relaxation are removed (compare Figs. 6 and 7), particularly in the region of 0.5 nm^{-1}. The scattering profile from the combined overlap/gap structure (Fig. 7 *e*) is now in reasonable agreement with the observed profile (Fig. 7 *f*).

An attractive feature of the multiple-start spiral model is that it provides a simple explanation for the observed linear mass profile of fibril tips (Holmes et al., 1992). Fibrils assembled in vitro have non-identical tip shapes, either extended α-tips or short β-tips. By scanning transmission electron microscopy, Holmes et al. (1992) showed that fibril mass per unit length increases linearly with distance from the tip, with α-tips growing at the rate of 17 molecules per D and β-tips growing at about 50 molecules per D. Such linear mass increments imply that tip shape is paraboloidal. In the multiple-start spiral model, each arm of the spiral increases in mass at the rate of 1 molecule per D, so tip shape is determined simply by the number of spirals.

A disadvantage of spiral structures is the difficulty in accounting for the observed discrete 8 nm increment in fibril diameters (Parry and Craig, 1994), an observation that is readily compatible with cylindrical structures (Hulmes, 1983). Therefore cylindrical structures were constructed with layers of compressed microfibrils, as above, and with their long axes oriented in a radial direction (Fig. 8). The interlayer spacing (d) and intermicrofibril spacing within a layer (a) were calculated on the basis that the number of microfibrils in layer m was 9m, and the packing density throughout the fibril was the same as in the quasi-hexagonal lattice (0.49 molecules nm^{-2}; Hulmes and Miller, 1979). At large radius, the number of additional microfibrils per layer is $2\pi d/a$ (by analogy with the Galloway (1985) model), and the area per microfibril is $d \times a$. As the area per microfibril

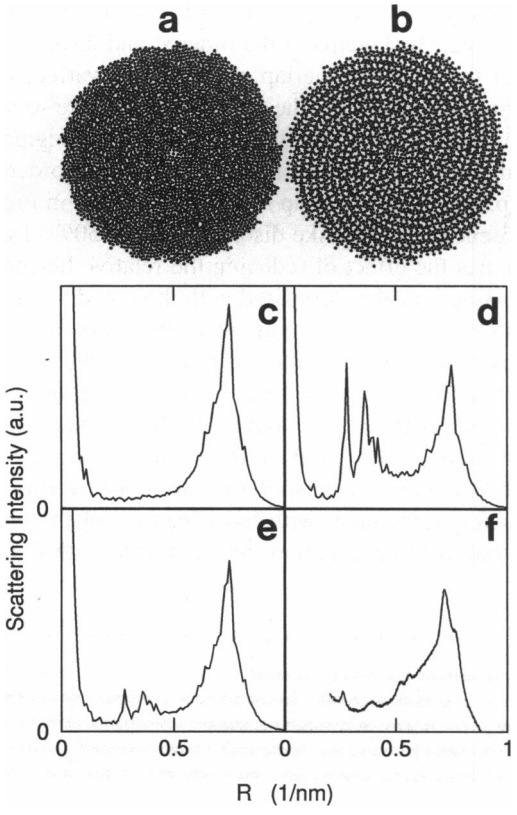

FIGURE 7 Energy-minimized spiral structure with radial molecular packing. The spiral model of the overlap region (Fig. 6 *a*) was subjected to energy minimization using the Lennard-Jones potential (see text) resulting in (*a*). To generate the gap region (*b*), molecular segments of length 0.5 D (identified in Fig. 6) were removed, without further energy minimization. The spiral structure is no longer apparent in the overlap region but is clearly retained in the gap region. Rotationally averaged theoretical scattering intensity profiles for the overlap and gap regions are shown in (*c*) and (*d*), respectively. The predicted scattering profile for the combined gap/overlap structure is shown in (*e*), with the observed equatorial x-ray diffraction pattern in (*f*). Calculated scattering profiles are on the same absolute scale.

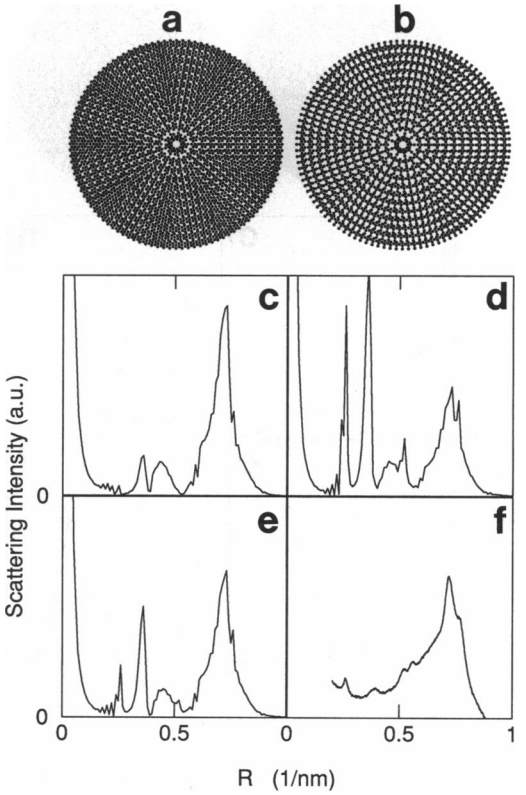

FIGURE 8 Cylindrical model with radial molecular packing. The model consists of concentric layers of radially oriented compressed microfibrils. The radial distance between adjacent layers converges to 3.8 nm, and the number of additional microfibrils per layer is 9 (see text). Rotationally averaged theoretical scattering intensity profiles for the overlap (*a*) and gap (*b*) regions are shown in (*c*) and (*d*), respectively. The predicted scattering profile for the combined gap/overlap structure is shown in (*e*), with the observed equatorial x-ray diffraction pattern in (*f*). Calculated scattering profiles are on the same absolute scale.

is known from the packing density, the choice of nine additional microfibrils per layer ensures that d and a approach asymptotic limits of 3.799 and 2.653 nm, respectively, both of which are within 0.5% of the corresponding spacings in the quasi-hexagonal lattice. The theoretical scattering profiles (Fig. 8, *c–e*) show a combination of sharp peaks at low angles and a broad maximum at about 0.75 nm^{-1}. Again, some unacceptable molecular overlaps were present in the geometrically determined structure, which were removed by energy minimization (Fig. 9). After relaxation, regions of crystallinity maintained their ordered appearance, while grain boundaries between crystalline domains became more defined. These features, together with the radial orientation of the 3.8 nm spacing (Fig. 9 *b*) are consistent with electron microscopy and image processing of collagen fibril transverse sections (Hulmes et al., 1981, 1985). The theoretical scattering profile of the combined overlap/gap structure (Fig. 9 *e*) is also very similar to the observed x-ray diffraction data (Fig. 9 *f*).

To refine the agreement between the observed and calculated x-ray scattering profiles for the energy-minimized radially packed cylindrical model (Fig. 9), various combinations were made with regions of disordered, liquid-like packing (Fig. 2). From the calculated scattering profiles, it is clear that the main contribution to the sharp maxima in the low-angle equatorial diffraction pattern is from the gap region, because of the inherently high contrast imposed by the gaps. The gap region is also likely to be more disordered, however, as a result of the relatively low packing density, compared with the overlap region. The transition from the relatively ordered overlap region to the relatively disordered gap region will not be abrupt, and it seems likely that the order in the overlap region will impose some order in the gap region in the vicinity of the gap/overlap interface. In addition, it is likely that different parts of the gap and overlap regions will differ in their extents of long-range lateral order as a result of amino acid sequence-specific intermolecular interactions. Covalent cross-linking, which occurs in the region of the gap/overlap interface, may also impose additional long-range order. Therefore we defined four regions in the D repeat (Fig. 10): 1) disordered (Fig. 2) partial gap region, 2) disordered (Fig. 2) partial overlap region, 3) relatively ordered (Fig. 9) N-terminal gap/overlap interface region, and 4) relatively ordered (Fig. 9) C-terminal gap/overlap interface region. The lengths of the ordered and disordered sections of the gap and overlap regions were varied, and the scattering intensity from the composite structure was calculated by adding the intensity from the interface regions (calculated coherently) to the intensities from the disordered partial gap, and partial overlap regions. As shown in Fig. 11 *b*, the presence of liquid-like disorder in, e.g., 50% of the gap region, has the effect of reducing the relative height of the sharp (Bragg) peaks, compared with the broad maximum at 0.75 nm^{-1}. The broad maximum in the theoretical profile remains relatively symmetrical, however, when compared with the observed profile (Fig. 11 *d*). To introduce the required asymmetry while maintaining the height of the sharp (Bragg) peaks relative to the diffuse scatter, it was necessary to introduce liquid-like disorder in part of the overlap region. Satisfactory agreement with most features of the observed equatorial diffraction pattern was obtained with liquid-like

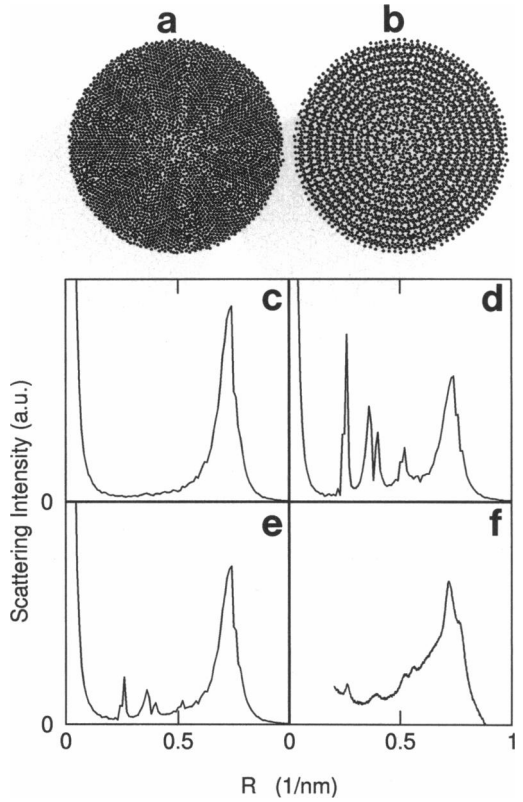

FIGURE 9 Energy-minimized cylindrical structure with radial molecular packing. The cylindrical model of the overlap region (Fig. 8*a*) was subjected to energy minimization using the L-J potential (see text) resulting in (*a*). To generate the gap region (*b*), molecular segments of length 0.5 D (identified in Fig. 8) were removed without further energy minimization. Peaks in Fig. 8, *c–e* are removed by the energy minimization. Rotationally averaged theoretical scattering intensity profiles for the overlap and gap regions are shown in (*c*) and (*d*), respectively. The predicted scattering profile for the combined gap/overlap structure is shown in (*e*), with the observed equatorial x-ray diffraction pattern in (*f*). Calculated scattering profiles are on the same absolute scale.

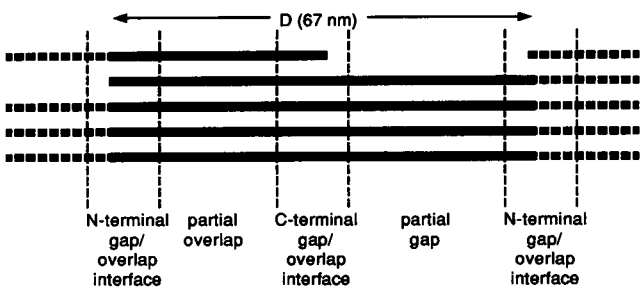

FIGURE 10 Diagram of a single D repeat in the collagen fibril showing the partial gap region, the partial overlap region and the N- and C-terminal gap/overlap interfaces. Each thick line represents the path of part of a collagen molecule (shown dotted in adjacent D repeats). The gap/overlap interfaces are the relatively ordered high-contrast regions that are thought to contribute most to the sharp (Bragg) maxima in the low-angle, equatorial x-ray diffraction pattern.

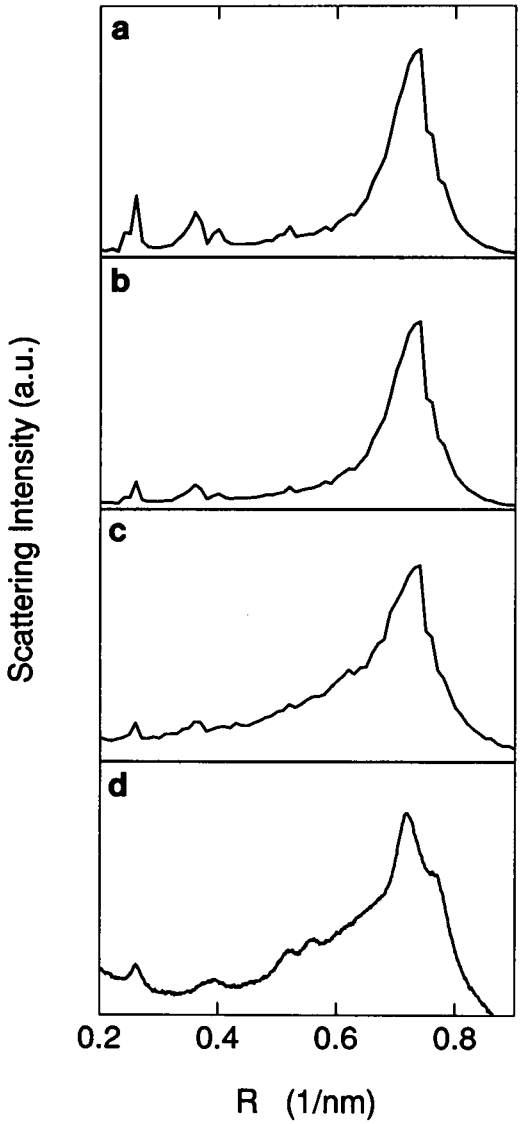

FIGURE 11 Scattering profiles for composite structures with liquid-like disorder (HD model) in the partial gap and overlap regions, and long-range order (relaxed radially packed cylindrical model) in the gap/overlap interfaces (see Fig. 10). (*a*) Theoretical equatorial diffraction pattern from the relaxed radially packed cylindrical model throughout both gap and overlap regions (Fig. 9 *e*). (*b*) Calculated scattering intensity for a composite structure with liquid-like disorder (Fig. 2 *b*) in 50% of the gap region, with the rest of the structure as in (*a*). (*c*) calculated scattering intensity for a composite structure with liquid-like disorder (Fig. 2, *a* and *b*) in 60% of the overlap region and in 80% of the gap region, with the rest of the structure (the gap/overlap interfaces) as in (*a*). In the composite structures (*b* and *c*), the scattering intensity from the relatively ordered interface regions was calculated coherently and added, incoherently, to the intensity from the disordered region(s). (*d*) Observed equatorial x-ray diffraction pattern from rat tail tendon.

disorder in 80% of the gap region and in 60% of the overlap region, as shown in Fig. 11 *c*.

CONCLUSIONS AND PERSPECTIVES

Fig. 12 shows an enlarged view of the relaxed, radially packed cylindrical structure (Fig. 9).

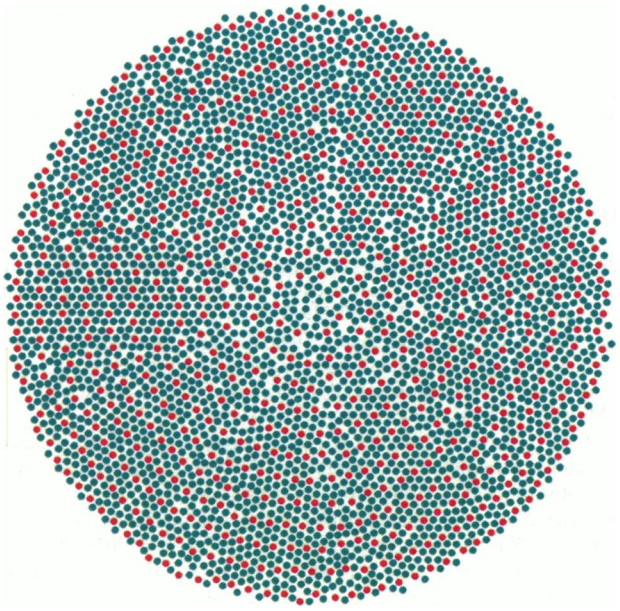

FIGURE 12 Enlarged view of the relaxed, radially packed cylindrical structure (Fig. 9). The molecular arrangement in the overlap region is shown, with one molecular segment (e.g., number 1; see Fig. 5) indicated in red.

There is a limit to the extent that the above relatively simple considerations can account for all the details of the observed equatorial x-ray diffraction pattern of tendon collagen. For example, the energy minimization takes no account of the anisotropy in intermolecular interactions. Molecules were approximated as cylinders; a more detailed model would require consideration of interactions between amino acid residues arranged on the collagen triple helix. In addition, the different packing densities between gap and overlap regions suggests possible differences in molecular mobility, as indicated by the work of Fraser et al. (1987). The effects of molecular mobility were not considered here (all the structures were instantaneous "snapshots"), and this will alter the relative contributions of the gap and overlap regions. A further consideration is the effect of fibril size, here limited to a diameter of 50 nm. Fibril diameter may be an important parameter in determining the extent of crystallinity in a fibril, with consequent effects on the x-ray diffraction pattern.

This is the first attempt to account for all the features of both the x-ray diffraction and electron microscope data in a single model for the molecular packing in collagen fibrils. Closest agreement was obtained for the radially packed cylindrical model, with additional liquid-like disorder in both the gap and overlap regions. We feel that the general features of this model may serve as a starting point for future refinements, as outlined above. Considerations of statistical thermodynamics, as illustrated here, will have to enter into any further mathematical modeling of both short- and long-range order in collagen fibrils.

This work was supported by the Biology and Biotechnology Science Research Center (TJW) and the Wellcome Trust (Research Leave Fellowship

to DJSH). We wish to thank L. Wess and staff of the BBSRC Daresbury SRS Laboratory for assistance on beamline 7.2. PF was supported by a visiting fellowship from the Science and Engineering Research Council. We are grateful to H. Jakob for providing a computer program for Monte Carlo simulations of the L-J potential, and to A. Miller, R. D. B Fraser, and J. Squire for discussions.

REFERENCES

Abraham, F. F. 1981. The phases of two dimensional matter, their transitions and solid state stability. A perspective via computer simulation of simple atomic systems. *Phys. Rep.* 80:339–374.

Birk, D. E., and T. F. Linsenmayer. 1994. Collagen fibril assembly, deposition, and organization into tissue-specific matrices. *In* Extracellular Matrix Assembly and Structure. P. D. Yurchenco, D. E. Birk, and R. P. Mecham, editors. Academic Press, San Diego. 91–128.

Brodsky, B., and E. F. Eikenberry. 1982. Characterization of fibrous forms of collagen. *In* Methods in Enzymology, Vol. 82. L. Cunningham and D. Fredriksen, editors. Academic Press, New York. 127–174.

Chapman, J. A. 1989. The regulation of size and form in the assembly of collagen fibrils in vivo. *Biopolymers.* 28:1367–1382, 2201–2205.

Eikenberry, E. F., B. Childs, S. B. Sheren, D. A. D. Parry, A. S. Craig, and B. Brodsky. 1984. Crystalline structure of type II collagen in lamprey notochord sheath. *J. Mol. Biol.* 176:261–277.

Franc, S. J. 1993. Ultrastructural evidences of a distinct axial domain within native rat tail tendon collagen fibrils. *Submicrosc. Cytol. Pathol.* 25: 85–91.

Fraser, R. D. B., T. P. MacRae, and A. Miller. 1987. Molecular packing in type I collagen fibrils. *J. Mol. Biol.* 193:115–125.

Fraser, R. D. B., T. P. MacRae, A. Miller, and E. Suzuki. 1983. Molecular conformation and packing in collagen fibrils. *J. Mol. Biol.* 167: 497–521.

Fratzl, P., N. Fratzl-Zelman, and K. Klaushofer. 1993. Collagen packing and mineralization. *Biophys. J.* 64:260–266.

Galloway, J. 1985. Structure of collagen fibrils. *In* Biology of Invertebrate and Lower Vertebrate Collagens. A. Bairati and R. Garrone, editors. Plenum Publishing Corp., New York. 73–82.

Grynpas, M. 1977. Three dimensional packing of collagen in bone. *Nature.* 265:381–382.

Hodge, A. J., and J. A. Petruska. 1963. Recent studies with the electron microscope on ordered aggregates of the tropocollagen macromolecule. *In* Aspects of Protein Structure. G. N. Ramachandran, editor. Academic Press, New York. 289–300.

Holmes, D. F., J. A. Chapman, D. J. Prockop, and K. E. Kadler. 1992. Growing tips of type I collagen fibrils formed in vitro are near paraboloidal in shape implying a reciprocal relationship between accretion and diameter. *Proc. Natl. Acad. Sci. USA.* 89:9855–9859.

Hukins, D. W. L., and J. Woodhead-Galloway. 1977. Collagen fibrils as examples of smectic A biological fibres. *Mol. Cryst. Liq. Cryst.* 41:33–39.

Hulmes, D. J. S. 1983. A possible mechanism for the regulation of collagen fibril diameter in vivo. *Coll. Rel. Res.* 3:317–321.

Hulmes, D. J. S. 1992. The collagen superfamily: diverse structures and assemblies. *Essays Biochem.* 27:49–647.

Hulmes, D. J. S., D. F. Holmes, and C. Cummings. 1985. Crystalline regions in collagen fibrils. *J. Mol. Biol.* 184:473–477.

Hulmes, D. J. S., J.-C. Jesior, A. Miller, C. Berthet-Colominas, and C. Wolff. 1981. Electron microscopy shows periodic structure in collagen fibril cross-sections. *Proc. Natl. Acad. Sci. USA.* 78:3567–3571.

Hulmes, D. J. S., and A. Miller. 1979. Quasi-hexagonal molecular packing in collagen fibrils. *Nature.* 282:878–880.

Jelinski, L. W., C. E. Sullivan, and D. A. Torchia. 1980. ^{2}H NMR study of molecular motion in collagen fibrils. *Nature.* 284:531–534.

Jesior, J. C., A. Miller, and C. Berthet-Colominas. 1980. Crystalline three dimensional packing is a general characteristic of type I collagen fibrils. *FEBS Lett.* 113:238–240.

Jones, E. Y., and A. Miller. 1991. Analysis of structural design features in collagen. *J. Mol. Biol.* 218:209–219.

Katsura, N., T. Osamu, and M. Yokoyama. 1991. Three dimensional structure of type I collagen and mineralization. *Connect. Tissue.* 22:92–98.

Luft, J. H. 1971. Ruthenium red and violet II fine structural location in animal tissue. *Anat. Rec.* 171:369–416.

Mayne, R., and R. G. Brewton. 1993. New members of the collagen superfamily. *Curr. Opin. Cell Biol.* 5:883–90 .

Miller, A. 1976. Molecular packing in collagen. *In* Biochemistry of Collagen. G. N. Ramachandran and A. H. Reddi, editors. Plenum Publishing Corp., New York. 85–136.

Nakao, K., and R. I. Bashey. 1972. Fine structure of collagen fibrils as revealed by ruthenium red. *Exp. Mol. Pathol.* 17:6–13.

Parry, D. A. D., and A. S. Craig. 1984. Growth and development of collagen fibrils in connective tissues. *In* Ultrastructure of the Connective Tissue Matrix. A. Ruggeri and P. M. Motta, editors. Martinus Nijhoff, Boston. 34–64.

Piez, K. A., and B. L. Trus. 1981. A new model for packing of type I collagen molecules in the native fibril. *Biosci. Rep.* 1:801–810.

Ramachandran, G. N., and V. Sasisekharan. 1956. Cylindrical lattice structures of collagen. *Arch. Biochem. Biophys.* 63:255–268.

Raspanti, M., V. Ottani, and A. Ruggeri. 1989. Different architectures of the collagen fibril: morphological aspects and functional implications. *Int. J. Biol. Macromol.* 11:367–371.

Ruggeri, A., F. Benazzo, and E. Reale. 1979. Collagen fibrils with straight and helicoid microfibrils: a freeze fracture and thin section study. *J. Ultrastruct. Res.* 68:101–108.

Sasisekharan, V., and G. N. Ramachandran. 1957. Studies on collagen. II. Cylindrical lattice structure of collagen. *Proc. Ind. Acad. Sci. A.* 45:363–378.

Silver, D., J. Miller, R. Harrison, and D. J. Prockop. 1992. Helical model of nucleation and propagation to account for the growth of type I collagen fibrils from the symmetrical pointed tips: a special example of self assembly of rod like monomers. *Proc. Natl. Acad. Sci. USA.* 89:9860–9864.

Torchia, D. A. 1982. Solid-state NMR studies of molecular motion in collagen fibrils. *In* Methods in Enzymology, Vol. 82. L. Cunningham and D. Fredriksen, editors. Academic Press, New York. 174–186.

Woodhead-Galloway, J., and P. Machin. 1976. Modern theories of liquids and the diffuse equatorial x-ray scattering from collagen. *Acta Cryst.* A 32:368–372.

van der Rest, M. and R. Garrone. 1991. Collagen family of proteins. *FASEB J.* 5: 2814–2823.